Effect of solar chromospheric neutrals on equilibrium field structures

T. D. Arber, G. J. J. Botha and C. S. Brady
Centre for Fusion, Space and Astrophysics, Physics Department, University of Warwick, Coventry CV4 7AL, UK
T.D.Arber@warwick.ac.uk
G.J.J.Botha@warwick.ac.uk

ABSTRACT

Solar coronal equilibrium fields are often constructed by nonlinear force-free field (NLFFF) extrapolation from photospheric magnetograms. It is well known that the photospheric field is not force-free and the correct lower boundary for NLFFF construction ought to be the top of the chromosphere. To compensate for this, pre-filtering algorithms are often applied to the photospheric data to remove the non-force-free components. Such pre-filtering models, while physically constrained, do not address the mechanisms that may be responsible for the field becoming force-free. The chromospheric field can change through, for example, field expansion due to gravitational stratification, reconnection or flux emergence. In this paper we study and quantify the effect of the chromospheric neutrals on equilibrium field structures. It is shown that, depending on the degree to which the photospheric field is not force-free, the chromosphere will change the structure of the equilibrium field. This is quantified to give an estimate of the change in α profiles one might expect due to neutrals in the chromosphere. Simple scaling of the decay time of non-force-free components of the magnetic field due to chromospheric neutrals is also derived. This is used to quantify the rate at which, or equivalent at which height, the chromosphere is expected to become force-free.

Subject headings: MHD — Sun: chromosphere — Sun: activity — Sun: magnetic fields

1. Introduction

Magnetic fields emerge from the solar convection zone and through the photosphere in a non-force-free state. As they move through the chromosphere, these structures rearrange themselves to become force-free or potential by the time they reach the corona. In many studies of the overlying corona it is useful to construct the equilibrium magnetic field. Since the corona is low β, the coronal field is expected to be force-free. The natural choice for extrapolating the coronal field is therefore to use NLFFF models (Metcalf et al. 2008). Such models require the lower boundary to be consistent with the force-free approximation, i.e. exerts no stresses in the boundary, or more formally that the bottom boundary field fulfills several integral relations (Molodenskii 1969). Unfortunately the magnetic field is usually routinely measured with high accuracy only in the photosphere. The field there is not force-free and so it is common to apply a pre-filtering to these fields (Wiegelmann et al. 2008) to reproduce the force-free field one ought to see at the top of the chromosphere. Such pre-filtering techniques are constrained by physics, but do not directly address the physical processes responsible for the field becoming force-free as it crosses the chromosphere. Possible mechanisms include the expansion of the

The Astrophysical Journal, 705:1183–1188, 2009; doi:10.1088/0004-637X/705/2/1183

flux due to gravitational stratification, the field moving up into a low β plasma and thus expanding to force-free through the dominant Lorentz force or reconnection. These mechanisms are certainly all active in the chromosphere, but in this paper we concentrate solely on the effect of neutrals on the field structure.

The photosphere and chromosphere are weakly ionized plasmas. It has been shown (Goodman 2000; Khodachenko et al. 2004) that the presence of neutrals can give rise to a significant anisotropy in the plasma resistivity in the solar atmosphere. The dominant term in the mid to upper chromosphere is the Cowling resistivity (Cowling 1957; Braginskii 1965) that only acts on perpendicular current and that has been shown to have a significant effect on emerging magnetic flux (Leake & Arber 2006; Arber et al. 2007). This resistivity, which is due to ion-neutral collisions, acts to dissipate currents perpendicular to the magnetic field but does not directly affect parallel current. It therefore acts to drive the magnetic field configuration towards force-free. Note however that the form of the Cowling resistivity is such that it cannot be expanded out into the standard diffuse form in the induction equation - a point which will become important later in this paper. To estimate the importance of this effect on the structure of equilibrium fields, we study the change in equilibria for idealised current sheets. Throughout we deal with just 1D current sheets, i.e. there is only one non-ignorable coordinate, and quantify how these current sheets change when a Cowling resistivity of chromospheric magnitude is applied. Specifically we quantify the change in the α profile, where we define α through the decomposition of current density through

$$\mathbf{j} = \frac{\alpha(\mathbf{r})\mathbf{B}}{\mu_0} + \mathbf{j}_\perp \tag{1}$$

where $\mathbf{j}_\perp$ is the current density perpendicular to the magnetic field $\mathbf{B}$. As one might expect, the Cowling resistivity acts to dissipate $\mathbf{j}_\perp$, but in so doing it also changes the distribution of $\alpha(\mathbf{r})$. It is this change in $\alpha(\mathbf{r})$, and the timescale for that change, that is calculated in this paper. An earlier study by (Burnette et al. 2004) showed the best fit of the linear force-free α found from photospheric measurements and the coronal field above that active region are in agreement. In this context best fit means that the force-free field captures the general features of the overlying corona. This was shown to be consistent with taking the un-weighted average of the measured photospheric $\alpha(x, y)$ over the domain of interest, where (x, y) are coordinates in the photospheric plane.

The effect of Cowling resistivity on current sheets has been studied before for interstellar gases (Heitsch & Zweibel 2003; Brandenburg & Zweibel 1994) but always in terms of its effect on reconnection. For these studies a reconnection rate is estimated under the assumption that any ion reaching the reconnection site recombines to form a neutral atom. For chromospheric plasmas the ionisation state is maintained through a combination of many processes, for example radiative transport, conduction and shock heating. In our study the degree of ionisation is a function of height only and we therefore solve the full set of equations for a partially ionized plasma. Here we concentrate only on the change in equilibrium field as a result of introducing neutrals and specifically only for those plasma parameters expected in the solar chromosphere.

2. Model

We solve the full, time-dependent set of resistive MHD equations with an anisotropic resistivity such that

$$\frac{\partial \rho}{\partial t} = -\nabla \cdot (\rho \mathbf{v}) \tag{2}$$

$$\frac{\partial (\rho \mathbf{v})}{\partial t} = -\nabla \cdot (\rho \mathbf{v}\mathbf{v}) + \mathbf{j} \times \mathbf{B} - \nabla P + \nabla \cdot \mathbf{S} \tag{3}$$

$$\frac{\partial \mathbf{B}}{\partial t} = \nabla \times (\mathbf{v} \times \mathbf{B}) - \nabla \times (\eta_\parallel \mathbf{j}_\parallel) - \nabla \times (\eta_\perp \mathbf{j}_\perp) \tag{4}$$

$$\frac{\partial (\rho \epsilon)}{\partial t} = -\nabla \cdot (\rho \epsilon \mathbf{v}) - P \nabla \cdot \mathbf{v} + \eta_\parallel j_\parallel^2 + \eta_\perp j_\perp^2 + \zeta_{ij} S_{ij} \tag{5}$$

and with Ohm's law

$$\mathbf{E} + \mathbf{v} \times \mathbf{B} = \eta_\parallel \mathbf{j}_\parallel + \eta_\perp \mathbf{j}_\perp, \tag{6}$$

where all the symbols have the same meaning as in (Leake & Arber 2006). The stress tensor $\mathbf{S}$ has components $S_{ij} = \nu[\zeta_{ij} - (\delta_{ij}\nabla \cdot \mathbf{v})/3]$ and $\zeta_{ij} = (\partial v_i/\partial x_j + \partial v_j/\partial x_i)/2$. Note that in this model the plasma pressure is given by

$$P = \frac{\rho k_B T}{\mu_m} \tag{7}$$

and the specific internal energy density by

$$\epsilon = \frac{P}{\rho(\gamma - 1)} + (1 - \xi_n)\frac{X_i}{\bar{m}} \tag{8}$$

where $\bar{m}$ is the average ion mass, ξ_n is the fraction of the local total mass density that is neutral hydrogen and X_i is the ionization energy of hydrogen. Since we are dealing with a partially ionized plasma, the reduced mass μ_m is given by $\mu_m = \bar{m}/(2-\xi_n)$. Some simulations of the chromosphere model ionization and radiative transport by fixing γ. Here we use $\gamma = 5/3$ with ionization effects included through the ξ_n dependence of μ_m. We do not include either the heating or loss terms which would maintain the chromospheric temperature in a completely self-consistent treatment. Instead we look only at processes which do not significantly affect the local temperature, thus keeping ξ_n fixed as a function of height above the photosphere.

A full treatment including all terms in the Ohm's law, with neutrals and finite Larmor radius effects, introduces many more terms than presented in Equation (6). Some of these terms can be used to express the plasma resistivity, or alternatively the conductivity, as a tensor (Goodman 2000). The anisotropic form of Ohm's law used here are just the leading order terms required for an accurate treatment of the mid to upper chromosphere, as demonstrated in (Khodachenko et al. 2004).

Here we concentrate on 1D current sheets of the form

$$B_z(x) = -B_0 \tanh\left(\frac{x}{L}\right), \tag{9}$$

$$B_y(x) = bB_0/\cosh\left(\frac{x}{L}\right), \tag{10}$$

where the (x, y) plane is parallel to the photosphere and z represents height. These 1D computations use a Lagrangian-remap code (Arber et al. 2001) with a resolution of 8000 to 10000 grid cells. We model different width current sheets so the actual spatial resolution varies with problem size, but is always sufficient to accurately resolve the solution as verified by convergence tests. The time resolution is determined by the stability limit imposed by the resistive terms as described in (Leake & Arber 2006).

When $b = 1$ we recover the nonlinear force-free field used by (Yokoyama & Shibata 2001), while $b = 0$ gives the Harris current sheet. In this manner we regulate the amount of parallel and perpendicular current densities ($j_\parallel$ and $j_\perp$) in the system to obtain an intermediate current sheet, with $b = 1$ giving only $j_\parallel$ and no $j_\perp$, and $b = 0$ only $j_\perp$ and no $j_\parallel$. Equivalently b can be viewed as a parameter that measures the degree to which the magnetic field is force-free. When $b = 1$ the field is completely force-free and when $b = 0$ there is no force-free component. At $t = 0$ the system is in pressure balance, with gas pressure balancing magnetic pressure by a suitable density distribution and uniform temperature. In this equilibrium the z direction, i.e. vertical distance measured above the photosphere, is ignorable. Gravity therefore plays no role. The initial pressure balance is an MHD equilibrium and therefore only changes due to $\eta_\perp$ dissipating perpendicular current. Hence when $b = 1$, $\eta_\perp$ has no effect.

In the chromosphere Cowling resistivity is orders of magnitude larger than Spitzer resistivity. For this reason, as well as to isolate the effects of $\eta_\perp$, we set $\eta_\parallel = 0$. This means that only $\mathbf{j}_\perp$ is dissipated while $\mathbf{j}_\parallel$ is left intact. The Cowling resistivity is formulated as

$$\eta_\perp = B^2\eta_0, \tag{11}$$

where B^2 is the local magnetic field. The value of the constant η_0 is fixed at the value for Cowling resistivity one would obtain using densities and temperatures from the VAL-C model (Vernazza et al. 1981). Note that throughout this paper S.I. units are used and the resistivity is therefore in Ωm. By choosing a constant temperature, far field density and η_0, we essentially fix the temperature and density at a specific height above the photosphere. The expression used to evaluate the Cowling resistivity is

$$\eta_\perp = \frac{{\xi_n}^2 B^2}{\alpha_n} = \eta_0 B^2, \tag{12}$$

with

$$\alpha_n = \frac{1}{2}\xi_n(1 - \xi_n)\frac{\rho^2}{m_n}\sqrt{\frac{16k_B T}{\pi m_i}}\Sigma_{in} \tag{13}$$

where m_n and m_i are the effective neutral and ion masses, ξ_n is the neutral fraction described in (Leake & Arber 2006) and $\Sigma_{in} = 5 \times 10^{-19}\mathrm{m}^2$ is the ion-neutral collision cross-section. Thus η_0 is completely specified as a function of height from the VAL-C model and $\eta_\perp$ requires the local magnetic field strength in addition to VAL-C. Note that for a small neutral fraction the Cowling resistivity increases linearly with the concentration of neutrals. However as the limit $\xi_n \to 1$ is approached the resistivity becomes singular as $\xi_n/(1-\xi_n)$. This makes physical sense as a neutral gas cannot support currents and the singular resistivity only allows potential field solutions. The $\xi_n/(1-\xi_n)$ dependence does mean that the resistivity is sensitive to ξ_n when $\xi_n \simeq 1$. The scaling laws derived in this paper are typically for $\xi_n = 0.523$, which corresponds to the location at which the Cowling resistivity is a maximum in the VAL-C model. This is just below the transition region. When estimating timescales for other heights, and $\xi_n \simeq 1$, the value of ξ_n was calculated directly from VAL-C. The scaling relations we derive later give timescales that are only a function of $\eta_\perp$ and the scale-length of the current sheet. To apply these relations to other values of (ξ_n, T, ρ) one simply calculates $\eta_\perp$ from Equation (12). The VAL-C model has been updated (Avrett & Loeser 2008) and this does change the height dependence of $\eta_\perp$. However, this has no effect on the scaling relations and their functional dependence on $\eta_\perp$, presented in this paper.

It should be noted that in this paper a current sheet with neutrals should not be confused with neutral current sheets in the MHD literature. Any current sheet with zero magnetic field at its centre, the so-called neutral line, is often called a neutral current sheet. This has nothing to do with the possible presence of neutral atoms. In this paper whenever we use the term neutral it always refers to un-ionized gas.

3. Harris current sheet

For the Harris current sheet, i.e. $b = 0$ in Equation (10), all of the current is perpendicular to the local magnetic field away from $x = 0$. In the absence of magnetic field at $x = 0$, parallel and perpendicular cannot be defined. However at this point, due to the magnetic field dependence of $\eta_\perp$ in Equation (11), the Cowling resistivity is also zero. Since the Cowling resistivity will dissipate any perpendicular current, the only position which can maintain a current for the Harris current sheet is at $x = 0$. Thus while perpendicular current is being dissipated, the current density at $x = 0$ is increasing. This can be seen in Figure 1, which shows the initial current density and its distribution 43 seconds later. This value was obtained using $B_0 = 1.75 \times 10^{-3}$ T and $L = 10^5$ m and VAL-C values for density and temperature at a height of 2.05 Mm. At this height $T = 7.66 \times 10^3$ K, $\rho = 1.802 \times 10^{-10}$ kg.m^{-3}, $\xi_n = 0.523$ and $\eta_\perp = 61.86$ Ωm. This height was chosen as it is at this height at which the Cowling resistivity is a maximum for the VAL-C model. Unless explicitly stated otherwise these are the default values used throughout this paper.

The characteristic time for the collapse of the current sheet down to $x = 0$ is $\tau = C\mu_0 L^2/\eta_\perp$ so that it scales as a diffusive process, as expected on dimensional grounds. Here C is a constant of proportionality that will be computer later. However the evolution, as can be seen in Figures 2 and 3, is not diffusive. An initial current sheet is known to diffuse away due to scalar resistivity, so that the current density at $x = 0$ varies as $1/(\eta t)^{1/2}$. With Cowling resistivity the current sheet grows to a singularity in finite time. This is the reverse for scalar resistivity, which starts with a singularity and diffuses it away. The assumption that the same similarity transformation is valid would therefore suggest a time dependence for the current density at $x = 0$ of $1/(\tau - t)^{1/2}$. This has been tested numerically with simulations stopped when the central current density concentration reaches grid scale - the final equilibrium can only be a δ function in current density for the Harris current sheet. Defining the collapse time as the time to reach grid scale gives a constant of proportionality of $C = 0.25 \pm 0.05$. Increasing the resolution does not change this estimate - as expected for collapse to a singular current sheet. The evolution of the maximum value of the current density and the full width half maximum (FWHM) of the current density distribution are shown in Figures 2 and 3. Despite the solution going to a current density singularity, the fluid velocities are always subsonic.

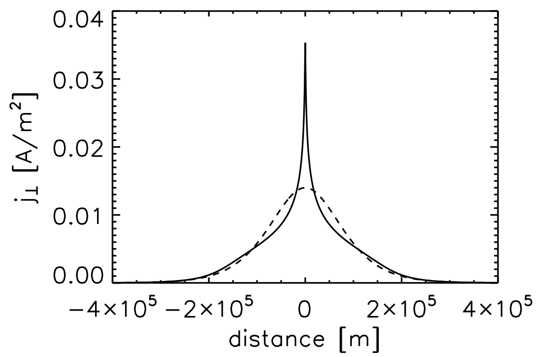

Fig. 1.— Perpendicular current density profiles at 43 seconds (solid line) and $t = 0$ (broken line) obtained with $\eta_\perp = 61.86\ \Omega$m for the Harris current sheet.

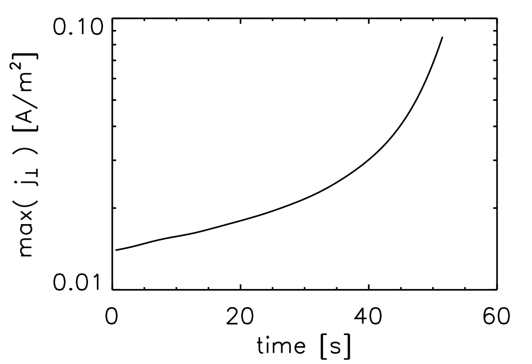

Fig. 2.— Time evolution of max($j_\perp$) for the same configuration as in Figure 1.

4. Current sheet with $j_\parallel \neq 0$

For $b \neq 0$ in Equation (10) the equilibrium contains some parallel current. In this case, while the Cowling resistivity dissipates $j_\perp$, it has no direct dissipative influence on $j_\parallel$. The initial conditions now contain a B_y field that is compressed as the current sheet collapses due to $\eta_\perp$. Consequently, the magnetic pressure builds up in the centre of the current sheet until a new equilibrium, without $j_\perp$, is established. As a result of this contraction of the current sheet width, the $j_\parallel$ is also concentrated in the centre although the total parallel current density is unaltered. Thus the Cowling resistivity removes $j_\perp$ and in so doing also alters the profile of the $j_\parallel$. This is shown in Figures 4 and 5. Although $j_\parallel$ is not dissipated (Figure 5), the α distribution changes shape with the changing current sheet width. In Figure 4 there is still some $j_\perp$ after 1000 seconds, but in the central region in which $j_\parallel$ is concentrated, this remaining $j_\perp$ has little effect on the field structure. Thus at this time of measuring α, the current sheet appears to be in equilibrium. These equilibria are approached asymptotically, so that the time dependence diminishes as the solution evolves. Throughout this process the fluid velocities remain subsonic, as in the case of the Harris current sheet.

Since the Cowling resistivity is not zero at $x = 0$, as was the case for the Harris current sheet, $j_\perp$ is always dissipated. Expecting the same similarity scaling with time therefore suggests a time dependence $j_\perp \propto \exp[-(t/\tau)^{1/2}]$, which has been tested numerically by fitting this functional form to simulation results for various L and $\eta_\perp$. An example of the simulation data and fitted function is shown in Figure 6. For all values of $\eta_\perp$ the r.m.s. error was $O(10^{-5})$A m^{-2} for typical perpendicular current densities of 2×10^{-3}A m^{-2}, i.e. a fractional error for each data point of approximately 10^{-2}. The same fractional accuracy was found for all fits in this paper.

In a similar way the time evolution of max(α) was fitted to the functional form

$$\alpha = \alpha_0 + (\alpha_\infty - \alpha_0)\left(1 - e^{-t/\tau}\right), \qquad (14)$$

where α_0 is the initial α measurement and α_∞ the value after infinite time, an example of which is shown in Figure 7. All values of $\eta_\perp$ gave a fractional r.m.s. error of $O(10^{-2})$. The same fractional error for the fit is found for values of length scales from $L = 1$ Mm to $L = 100$ m.

Once again it is found that $\tau = C\mu_0 L^2/\eta_\perp$ although now the typical value for the proportionality constant is $C = 1.9 \pm 0.1$, obtained from the scaling of $j_\perp$ for values of $0.1 \le b \le 1$. The scaling of $\max(\alpha)$ gives $C = 1.3 \pm 0.5$.

The FWHM of the α distribution decreases linearly in time and $\max(\alpha)$ increases exponentially. This is consistent with the total integrated α remaining constant, in agreement with (Burnette et al. 2004). Figures 8 and 9 show the changes in FWHM and $\max(\alpha)$ that have occurred after 400 seconds. While the local value of α at a particular location changes, the averaged value of α over the whole domain, denoted by $< \alpha >$, changes little. For $b = 0.1$ the change in $< \alpha > / < \alpha_0 >$ is 3%, while for $b = 0.25$ it is 0.1%, where $< \alpha_0 >$ is measured at $t = 0$. If more $j_\parallel$ is included (i.e. higher b values) the change becomes even smaller.

5. Variation of equilibration time with height

The presence of any $\eta_\perp$ is sufficient to force the above change in α, albeit on a slower timescale for lower values of $\eta_\perp$. This suggests that the equilibrium magnetic field must be force-free once a chromospheric region of significant $\eta_\perp$ is encountered, unless there are other drivers for the field. The absolute magnitude of $\eta_\perp$ is shown in Figure 1 of (Leake & Arber 2006), and on that scale is significant from about a height of 1 Mm above the photosphere. However the Cowling resistivity dominates over the parallel Spitzer value above a height of about 500 km. (See Figure 1 in (Khodachenko et al. 2004)). Taking model atmospheric values from the VAL-C model, $\eta_0(h = 500\text{ km})/\eta_0(h = 2\text{ Mm}) \simeq 10^{-5}$ suggests that the Cowling resistivity is unimportant at such low heights. Note that here η_0 is used in the comparison, as this depends only on the model atmosphere, i.e. dependence on the local magnetic field strength has been factored out.

The estimated timescale for current sheet collapse has been determined above for field configurations with some $j_\parallel$. The characteristic timescale for neutrals in the chromosphere to remove non-force-free components of the magnetic field was

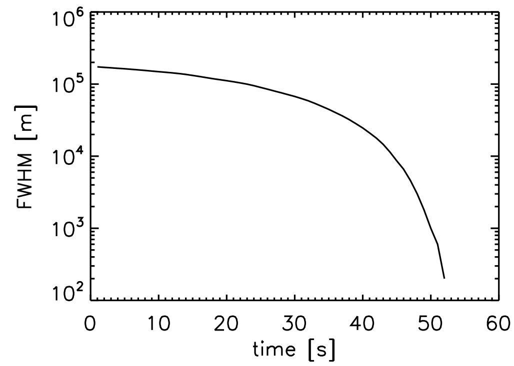

Fig. 3.— Time evolution of the FWHM of the perpendicular current density distribution, as depicted in Figure 1.

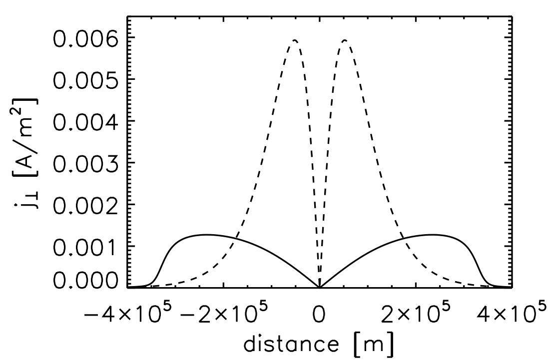

Fig. 4.— Profiles of $j_\perp$ at 1000 seconds (solid line) and at $t = 0$ (broken line) obtained with $\eta_\perp = 61.86\ \mathrm{m^2.s^{-1}}$ and $b = 0.5$ in Equation (10).

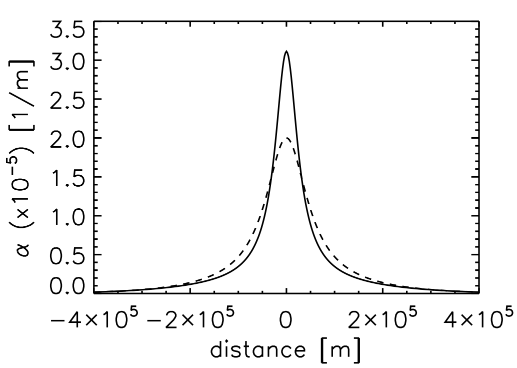

Fig. 5.— Profiles of $\alpha = \mu_0 j_\parallel / B$ measured as in Figure 4.

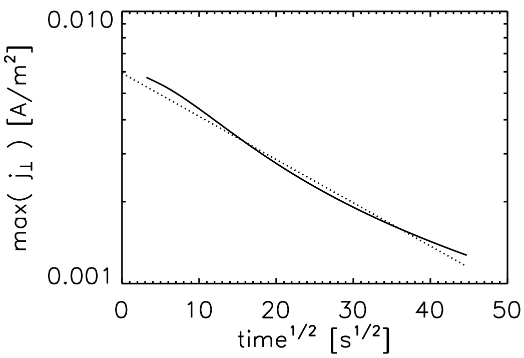

Fig. 6.— Fitting functional form $\exp(-\sqrt{t/\tau})$ (dotted line) to the time evolution of $\max(j_\perp)$ obtained with $b = 0.5$, $L = 10^5$ m and $\eta_0 = 30.93\ \Omega$m (solid line). The r.m.s. error is 8.0×10^{-6}A m^{-2} measured over 200 data points.

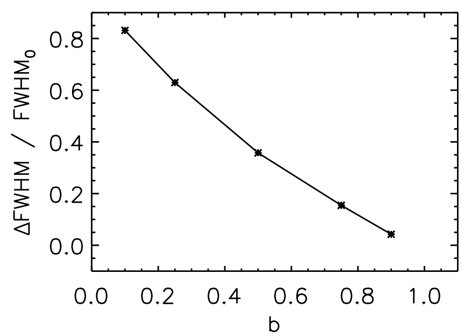

Fig. 8.— The change in the FWHM measurement as a function of b in Equation (10). $\triangle$FWHM $= |\mathrm{FWHM}_{400} - \mathrm{FWHM}_0|$, measured at 400 seconds and initialisation.

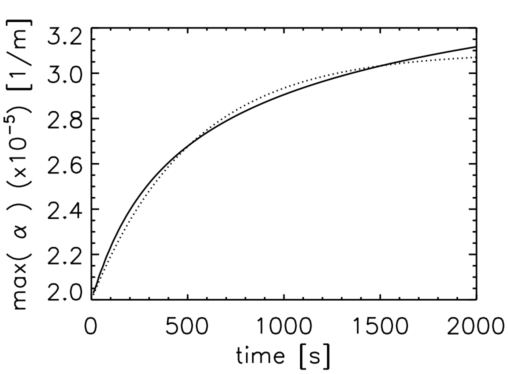

Fig. 7.— Fitting functional form (14) (dotted line) to the time evolution of $\max(\alpha)$ (solid line) obtained with the same parameters as in Figure 6. The r.m.s. error is 2.6×10^{-7}m^{-1} measured over 200 data points.

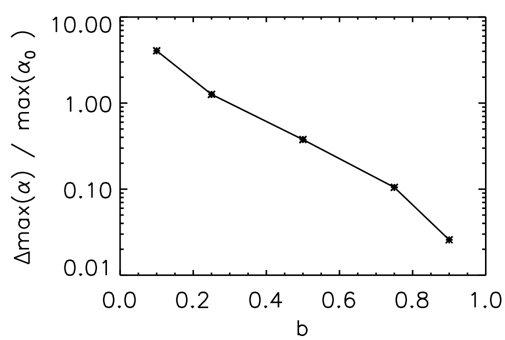

Fig. 9.— The change in $\max(\alpha)$ as a function of b. $\triangle \max(\alpha) = \max(\alpha_{400}) - \max(\alpha_0)$, measured at 400 seconds and initialisation. For $b = 1$ no change occurs.

found to be

$$\tau \simeq 2\frac{\mu_o}{\eta_0}\frac{L^2}{B^2}. \tag{15}$$

Since η_0 is a function of the height above the photosphere, h, this timescale can be written purely as a function of height if some prescription for $B(h)$ and $L(h)$ is given. As an example, choose a magnetic field that varies with height through $B(h) = B_p(\rho(h)/\rho_p)^{0.3}$ (Leake & Arber 2006), where subscript letter p refers to photospheric values. Starting with $B_p = 0.12$ T and using VAL-C for the density variation, this prescription gives a magnetic field in the corona of 10 G. The scale-length variation can then be fixed by assuming $L^2 = L_p^2 B_p/B(h)$ from flux conservation for a 2D field source. Fixing $B_p = 0.12$ T, Figure 10 (solid line) plots the decay timescale for non-force-free field structures as a function of height for $L_p = 10^4$ m. The values for other B_p and L_p can easily be determined from the scaling of τ. For the values in Figure 10, on a timescale of 2 minutes the magnetic field would become force-free at about 2 Mm, whereas over a timescale of 10 minutes the chromospheric field would be force-free by 800 km above the photosphere. These estimates of course assume that the chromosphere is not been driven on faster timescales, for example by flux emergence, and are therefore merely indicative of the timescales on which chromospheric neutrals tend to drive the magnetic field towards being force-free.

A limitation on this approach for estimating the timescale for the decay of non-force-free fields is the sensitivity to the model atmosphere. The original VAL-C model has been recently updated to the C7 model (Avrett & Loeser 2008). For comparison with the original VAL-C values, the dotted line on Figure 10 shows the same calculation with the improved C7 model. The shape of the timescale curve differs significantly, although the timescale at 800 km still remains about 10 minutes. Plots of the densities and temperatures show only slight variations between VAL-C and model C7 and so the differences shown in Figure 10 highlight the sensitivity of the results to the choice of atmospheric model. This sensitivity is due to the $\xi_n/(1-\xi_n)$ dependence of $\eta_\perp$ shown in Equation (12), so a few percent changes in (T, ρ) can change $\eta_\perp$ by a factor of order two. Despite this the estimated timescale is still given by Equation (15).

6. Conclusion

Under chromospheric conditions a 1D current sheet will collapse on a diffusive time scale, in the absence of a parallel current density ($j_\parallel$), to a field discontinuity. The presence of $j_\parallel$ inhibits total collapse and the current sheet moves asymptotically to an equilibrium state. These changes are most clearly seen in plots of the change of the maximum value of the α profile and its FWHM, as shown in Figures 8 and 9. The spatially averaged α shows very little change during the collapse. Thus the presence of chromospheric neutrals, which dissipates $j_\perp$, also affects the distribution of $j_\parallel$ and as a result the local α profile. If the extent to which the field entering the chromosphere is not force-free, as measured by the parameter b in Equation (10), is known, then Figures 8 and 9 give a prescription for the change in α due to neutrals alone, as expected from the photosphere up to the top of the chromosphere.

The tendency for chromospheric neutrals to contract, and in the case of the Harris current sheet collapse to a singular current density in finite time, means that Cowling resistivity may act to hasten the onset of reconnection in 2D and 3D configurations. It must be pointed out however, that the Cowling resistivity itself cannot directly effect the reconnection rate. It only acts on $j_\perp$ and therefore will always vanish at a stationary reconnection site.

An analytic solution for the decay of $j_\perp$ has not been found. For uniform scalar resistivity the decay of a current sheet varies as $1/t^{1/2}$. By assuming that the similarity transformation which leads to this $t^{1/2}$ dependence remains true for Cowling resistivity, we postulated that the Harris current sheet would collapse as $j_\perp \propto /(\tau - t)^{1/2}$ and tested this against simulations. It was shown that $\tau = 0.25\mu_0 L^2/\eta_\perp$. For current sheets with non-zero field at $x = 0$, the perpendicular current density always decays due to the presence of chromospheric neutrals. By analogy with scalar resistive decay we assumed $j_\perp \propto \exp(-(t/\tau)^{1/2})$ and found that in this case $\tau \simeq 2\mu_0 L^2/\eta_\perp$.

Choosing the VAL-C and improved C7 models as the reference atmospheres and picking a height dependence for the magnetic field and current sheet width, give τ as a function of height, as shown in Figure 10. While this figure is just for

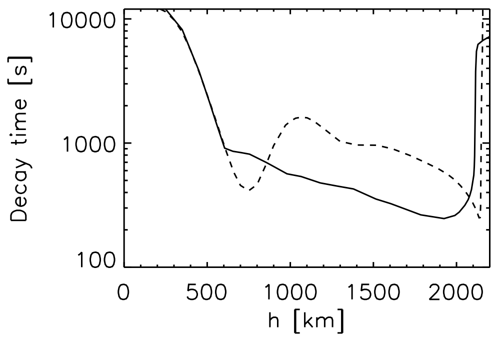

Fig. 10.— Variation of decay time τ for non-force-free components of the magnetic field as a function of height above the photosphere for $B_p = 0.12$ T and $L_p = 10^4$ m. Solid line is based on VAL-C. The dashed line on the updated C7 model.

a specific photospheric magnetic field and photospheric current sheet width, it does demonstrate clearly the height dependence of τ. If we assume an initially static, but not force-free, magnetic field and further assume the only perturbing influence on that field is the Cowling resistivity, then for the chosen values after $\simeq 10 - 20$ minutes the field above 800 km would have relaxed to NLFFF. Clearly there are a large number of assumptions required for this to be true. The chromosphere is dynamic with flux injection, photospheric driving, reconnection and spicules, all acting to perturb the magnetic field. What Figure 10 shows is the underlying tendency for the return to NLLFF configurations. Of course we have also assumed that the scalings tested here remain true for complex 3D fields. While on dimensional grounds alone this seems reasonable, this should be checked in later work.

The work was supported by an STFC grant. The computational work was supported by resources made available through Warwick University's Centre for Scientific Computing.

REFERENCES

Arber, T. D., Longbottom, A. W., Gerrard, C. L., & Milne, A. M. 2001, J. Comp. Physics, 171, 151

Arber, T.D., Haynes, M., & Leake, J.E. 2007, ApJ, 666, 541

Avrett, E. H. & Loeser, R., 2008, ApJS, 175, 229.

Braginskii, S.I. 1965, Transport processes in a Plasma, in Reviews of plasma physics, Vol. 1, (Consultants Bureau, New York)

Brandenburg, A., & Zweibel, E. G. 1994, ApJ, 427, L91

Burnette, A. B., Canfield, R. C., & Pevtsov, A. A. 2004, ApJ, 606, 565

Cowling T. G. 1957, MagnetoHydroDynamics, Monographs on Astronomical Subjects (Adam Hilger, Bristol, UK)

Goodman, M. L. 2000, ApJ, 533, 501

Heitsch, F., & Zweibel, E. G. 2003, ApJ, 590, 219

Khodachenko, M. L., Arber, T. D., Rucker, H. O., & Hanslmeier, A. 2004, A&A, 422, 1073

Leake, J. E., & Arber, T. D. 2006, A&A, 450, 805

Metcalf, T. R., DeRosa, M. L., Schrijver, C. J., Barnes, G., Van Ballegooijen, A. A., Wiegelmann, T., Wheatland, M. S., Valori, G., & McTiernan, J. M. 2008, Sol. Phys., 247, 269

Molodenskii, M. M. 1969, Soviet Astronomy, 12, 585

Vernazza, J. E., Avrett, E. H., & Loeser, R. 1981, ApJS, 45, 635

Wiegelmann, T., Thalmann, J. K., Schrijver, C. J., DeRosa, M. L., & Metcalf, T. R. 2008, Sol. Phys., 247, 249

Yokoyama, T., & Shibata, K. 2001, ApJ, 549, 1160